Neurobiology of Aging 76 (2019) 24–34

Contents lists available at ScienceDirect

Neurobiology of Aging

journal homepage: www.elsevier.com/locate/neuaging

Screening of a neuronal cell model of tau pathology for therapeutic compounds

Marcus Pickhardt [a,b,*], Michele Tassoni [c], Philip Denner [d], Birgit Kurkowsky [d], Ana Kitanovic [d], Christoph Möhl [d], Eugenio Fava [c,**], Eckhard Mandelkow [a,b,e,*]

[a] DZNE, German Center for Neurodegenerative Diseases, Bonn, Germany
[b] CAESAR Research Institute/Max-Planck-Inst., Bonn, Germany
[c] DZNE Systems Phenomics, Bonn, Germany
[d] DZNE Core Research Facilities and Services, Bonn, Germany
[e] Max-Planck-Inst. Metabolism Res, Hamburg Outstation @ DESY, Hamburg, Germany

ARTICLE INFO

Article history:
Received 19 September 2018
Received in revised form 23 November 2018
Accepted 30 November 2018
Available online 13 December 2018

Keywords:
Alzheimer
tau
Modulator
Cell screening
Pathway analysis
tau aggregation

ABSTRACT

We have developed a cell-based phenotypic automated high-content screening approach for N2a cells expressing the pro-aggregant repeat domain of tau protein (tau$^{RD\Delta K}$), which allows analysis of a chemogenomic library of 1649 compounds for their effect on the inhibition or stimulation of intracellular tau aggregation. We identified several inhibitors and stimulators of aggregation and achieved a screening reproducibility >85% for all data. We identified 18 potential inhibitors (= 1.1% of the library) and 10 stimulators (= 0.6% of the library) of tau aggregation in this cell model of tau pathology. The results provide insights into the regulation of cellular tau aggregation and the pathways involved in this process (e.g., involving signaling via p38 mitogen-activated protein kinase, histone deacetylases, vascular endothelial growth factor, rho/ROCK). For example, inhibitors of protein kinases (e.g., p38) can reduce tau aggregation, whereas inhibitors of deacetylases (histone deacetylases) can enhance aggregation. These observations are compatible with reports that phosphorylated or acetylated tau promotes pathology.

1. Introduction

tau (Microtubule-associated protein tau, Uniprot P10636) is a neuronal protein with multiple interactions to cytoskeletal elements and other cell components (Morris et al., 2011; Wang and Mandelkow, 2016). In a number of neurodegenerative diseases (termed tauopathies), tau undergoes pathological changes, most prominently by hyperphosphorylation and by forming insoluble fibrous aggregates (paired helical filaments and others; Goedert et al., 2012; Lee et al., 2001). For this reason, a major part of research on tau aims to analyze the factors that lead to pathological changes and to discover ways to prevent or reverse them.

To study tau aggregation on a cellular level, we have previously developed a tet-on inducible N2a cell line, which expresses the repeat domain of tau with the pro-aggregant frontotemporal dementia with parkinsonism mutation ΔK280 [four repeat tau (M) Q244-E372 with deletion of K280, 129 residues, termed tau$^{4RD\Delta K280}$, also known as K18$^{\Delta K}$ or tau$^{RD\Delta K}$] and develops aggregates within a few days (Khlistunova et al., 2006). Aggregation is toxic for this cell line (by lactate dehydrogenase and 3-(4,5-dimethylthiazol-2-yl)-2,5-diphenyltetrazolium bromide assays). As a control, the anti-aggregant variant tau$^{RD\Delta K_2P}$ (which contains proline inserts that prohibit beta structure and aggregation) does not aggregate and does not cause toxicity, thus providing evidence that the aggregation propensity of tau that is responsible for toxicity (Pickhardt et al., 2017). Treatment of this cell line with certain aggregation inhibitor compounds (resulting from an earlier screen of 200.000 compounds, Pickhardt et al., 2005) and with compounds screened for binding to monomeric tau (Pickhardt et al., 2015) showed that tau aggregation inhibitors (TAIs) have the ability to prevent toxicity and aggregation (Bulic et al., 2013). Similar rescue effects were observed for models of tauopathy derived from transgenic *Caenorhabditis elegans* or from organotypic slices of tau-transgenic mice (Dennissen et al., 2016; Fatouros et al., 2012). On the basis of these proof-of-principle results, we developed and validated a cellular phenotypic approach for an image-based data acquisition and data analysis, which quantify tau aggregation in an N2a cell model on

* Corresponding author at: Deutsches Zentrum für Neurodegenerative Erkrankungen e. V. (DZNE), Sigmund-Freud-Str. 27, 53127 Bonn, Germany. Tel.: +49 228 43302-543; fax: +49 228 43302-279.
** Corresponding author at: Deutsches Zentrum für Neurodegenerative Erkrankungen e. V. (DZNE), Sigmund-Freud-Str. 27, 53127 Bonn, Germany. Tel.: +49 228 43302-685; fax: +49 228 43302-279.
E-mail addresses: marcus.pickhardt@gmx.de (M. Pickhardt), eugenio.fava@dzne.de (E. Fava), eckhard.mandelkow@dzne.de (E. Mandelkow).

0197-4580/$ – see front matter © 2018 Elsevier Inc. All rights reserved.
https://doi.org/10.1016/j.neurobiolaging.2018.11.026

pharmacological standards. This high-content screening (HCS) assay was used to screen a chemogenomic library (composed of 1649 bioactive drugs, including 850 US Food and Drug Administration–approved compounds) for their effects on tau aggregation. The HCS assay was miniaturized (384-well format) and transferred to a robotic screening platform for fully automated and standardized processing. Automated image analysis routines were used to quantify tau aggregates by Thioflavin S staining and counterstaining of the nuclei by DRAQ5 and viability assays using resazurin (measuring the cellular amount of nicotinamidadenindinukleotid). Finally, data obtained from the validated hits were subject to chemogenomic and network analysis to determine the connections and the interactions of the small molecules with the annotated targets.

2. Results

2.1. Cells, screening workflow, image analysis

The initial steps were to optimize conditions for cell culture, cell density, plate format, and concentrations of the activation (Doxycycline and Cp16 [aminothienopyridazine, Ballatore et al., 2012]) and staining reagents (Thioflavin S and DRAQ5). For standardization, we used cells after passaging 3 times as the most effective procedure after reculturing of deep-freeze cell stabilates. This was performed at a density of 1.75×10^6 cells in 30 mL of minimum essential medium (MEM) in T150 flasks (Costar) for 84 hours. Under these conditions, the doubling time of the uninduced N2atau$^{RD\Delta K}$ cells was ~30 hours (data not shown). After harvesting, we determined the cell density and the ratio of living:dead cells, using a cell viability analyzer (Vi-Cell XR; Vi-CELL Reagent Pak [live:dead staining reagents] Beckman Coulter). The fraction of living cells was typically 85%–98% of the adherent cell population. A starting cell density of 6000 cells per well (384-well format) was optimal to create a sufficient cell layer after 48 h of incubation across the culture plate without detectable edge effects. The addition of Thioflavin S at a concentration of 12 μM (0.005%) simultaneously to the activation of tau$^{RD\Delta K}$ expression resulted in strong ThS-fluorescence of tau aggregates with a good signal-to-noise ratio (~10:1; ThS$^+$:ThS$^-$ cells) and no toxicity after 48 h, as reported previously (Pickhardt et al., 2017).

We established a cell-viability assay for the tau$^{RD\Delta K}$-N2a cells based on the reduction of resazurin ("Alamar Blue," blue) to resorufin (pink) by reduction equivalents like nicotinamidadenindinukleotid. The amount of resorufin as an indicator for cellular metabolism was measured by emission wavelength of 595 nm (excitation 535 nm). Several optimization steps for resazurin concentrations and incubation times were performed to achieve reducible signal intensities with a good signal-to-noise ratio (~6:1; N2a cells:cell-free medium) and minimal distribution effects (signal intensity variations over all 384 wells), leading to a standard application: 5 μM resazurin was added 1 hour before the fixation/nuclei-staining step to the cell media and incubated for 1 hour at 37 °C. Signal intensities were measured at 595 nm (exc. 535 nm), and the data were corrected by the background signal of cell-free media.

The initial screen was done with a chemogenomics library of 1649 bioactive drugs (Selleckchem). We treated the induced N2atau$^{RD\Delta K}$ cells with 1, 5, or 10 μM of the respective compound for 48 hours (Fig. 1A). Plates were seeded with 6000 cells per well in a 384-well format (step 1) and the activation solution [doxycycline + Cp16 (Ballatore et al., 2012) and ThS for staining of aggregating tau$^{RD\Delta K}$] was added (step 2) using a multidrop device. After transfer of the cell plates to a robotic platform, the library compounds were added in an automatic procedure (step 3) from preformed compounds spotting plates in different concentration ranges (Fig. 1A, day 1, a-c). After 48 hours of incubation, the N2a cells were fixed and their nuclei were stained in parallel by DRAQ5 (step 4). Finally, images were taken by an automated confocal microscope system (CellVoyager 6000, Yokogawa Ltd) where single N2atau$^{RD\Delta K}$ cells (Fig. 1B, red) and N2atau$^{RD\Delta K}$ cells containing tau aggregates (Fig. 1B, green/white) could be detected.

The image analysis was based mainly on cell detection defined by nuclei staining, the definition of the cell area (μm^2) and cell shape (ratio of width to length) (Fig. 1C), as well as the Thioflavin S fluorescence (Fig. 1D). The ratios of ThS$^+$ cells versus total cells were calculated for each well and normalized by the mean of the neutral controls (compound-untreated tau$^{RD\Delta K}$ expressing N2a cells). The result reflects the activity of a potential TAI or stimulator.

2.2. Distribution/reproducibility of data

The N2atau$^{RD\Delta K}$ cell line is positive for tau$^{RD\Delta K}$ expression in ~100% of the Dox-activated cells, as judged by antibody staining (K9JA/Cy5; Fig. S1A). The distribution of results (ratios of ThS$^+$ cells to all cells) for one of the screening runs is shown in Fig. 2. The green peak representing the positive (neutral) control (+Dox/Cp16, ThS$^+_{max}$ = 5%) and the mean was set to zero value as normalization point. Clearly separated from this, the negative (background) control is indicated by the dark blue peak (− Dox/Cp16, ThS$^+_{min}$ = 0.1%; +5.6× std). As an inhibitor control, we used 3 concentrations of compound BSc3094 (Pickhardt et al., 2007); their peaks are located between the peaks of neutral control and background control, indicating that the compound inhibits tau aggregation in a concentration-dependent manner (Fig. 2A, top). The reproducibility of the screening runs was ~86% (Fig. 2B).

2.3. Identification of self-fluorescent compounds

Some compounds can produce self-fluorescence in N2atau$^{RD\Delta K}$ cells although they show no fluorescence of in vitro emission screen. For example, treatment with rhodanine compounds (e.g., bb14; Bulic et al., 2007) developed a strong green fluorescence (~520 nm) of the whole cell population, independently of cellular tau aggregates (Fig. S1B and C). To avoid this phenomenon, we measured the Thioflavin S fluorescence at 2 excitation wavelengths (Fig. S1D–exc. 488 nm, Fig. S1E–exc: 405 nm). By changing the excitation to the lower wavelength of 405 nm, the total green fluorescence (at an emission 525 nm) drops down and the N2atau$^{RD\Delta K}$ cells with tau aggregates (white) and without (gray) are distinguishable. For the compound screening, we measured the green channel with both excitation wavelengths routinely. In the subsequent image analysis, we could identify such self-fluorescence compounds and exclude them from further testing.

2.4. Hit threshold, cell-viability threshold

Next, we established a routine analysis to set an unbiased threshold to identify hit compounds. We first collected all the data for the positive controls present in the screening and plotted their frequency distribution. We then calculated the fitted distribution of the positive control. From the fitted distribution, we chose 3× standard deviation as upper and lower thresholds for the hit selection. All data related to the compound-treated samples below the lower threshold were defined as inhibitors of tau aggregation, whereas data above the upper threshold were defined as stimulators of tau aggregation (Fig. S2B). Next, we analyzed the effect of the low molecular weight compounds in relation to cell viability. As in our phenotypic screen, we collected the information of the number of cells in each well and used this number as a proxy for cell viability. We defined 3 classes of results (toxic, mildly toxic, and

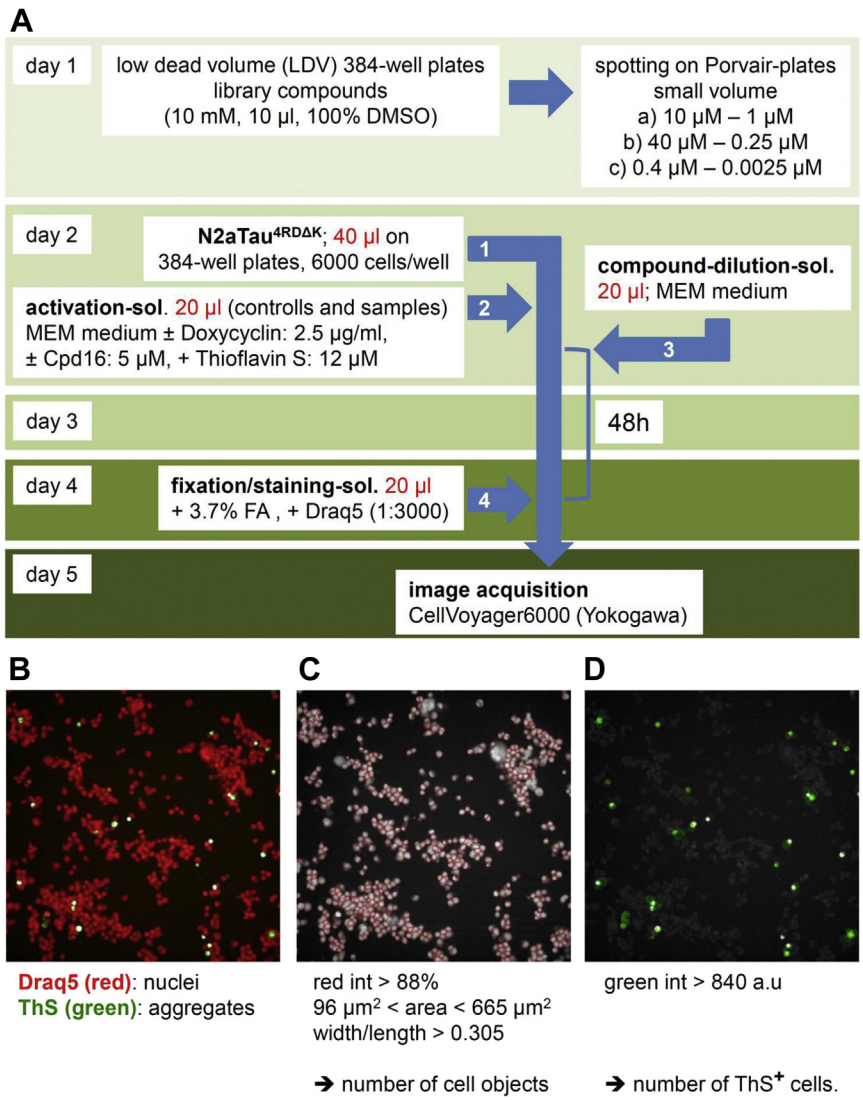

Fig. 1. Flow chart of the screening procedure and picture analysis. (A) Day 1: Spotting of compound library on 384-well library plates in the testing concentration range. Day 2: seeding of N2atau$^{RD\Delta K}$ cells on 384-well test plates; preparing control samples (neutral control: + Dox/Cp16 + Thioflavin S; background control: + Thioflavin S); preparing compound-testing samples: + Dox/Cp16 + Thioflavin S + transferring compounds from library plate to testing plate. Day 3: Incubation. Day 4: Fixation of cells on the test plates (37% formaldehyde) with simultaneous staining of nuclei (DRAQ5). Day 5: Image acquisition for ThS staining (cells with tau aggregates) and DRAQ5 (total cell count). (B) Images were analyzed by an automated image analysis routine on an analysis platform (Columbus vers. 2.4.1., Perkin Elmer), and the data were further quantified with a high-content assay analyzer (Genedata vers. 11.0.2., Genedata AG) regarding the total amount of cells (C) and the amount of ThS^{+} cells (D).

nontoxic; Fig. S2D). The distribution of the number of cells was clustered using a K-means algorithm that was able to divide the distribution into these 3 classes. Notably, all positive controls are contained in the nontoxic group (Fig. S2D, purple). Thus, our strategy for the hit selection was able to identify activators and inhibitors of tau aggregation in an unbiased manner, and for each of the compounds, the cell viability status was determined.

2.5. Primary hit selection (3 conc.)

The primary screening of 1649 bioactive drugs (Selleckchem) was performed at 3 concentrations (1, 5, and 10 µM) over an incubation period of 48 hours, and each data set was analyzed separately. We identified 182 potential inhibitors (Fig. S3A–E) and 225 stimulators (Fig. S3F–K) of tau aggregation with at least $\pm 3\times$ standard deviations separated from the normalized tau$^{RD\Delta K}$ expressing, compound-untreated control (neutral control). These compounds were grouped according to their cytotoxicity (not toxic, mildly toxic, and severely toxic) for aggregation inhibitors. Aggregation stimulators were all toxic in terms of decreasing the total cell count.

2.6. Dose-response (10 conc.), cluster analysis of tau modulators

Based on the results of the primary screen, the inactive compounds were excluded, whereas a subset of 361 compounds (182 inhibitors and additional 30 stimulators with the highest activity in the primary screen) were further retested in a dose-response (DR) manner in a concentration range of 0.25–40 µM (Fig. 3). For the stimulatory compounds, we were mainly interested in the strongest effects on tau aggregation in N2atau$^{RD\Delta K}$ cells. This allowed us to classify the compounds in several subgroups depending on their inhibitory or activation effects on tau aggregation and their cell toxicity. For this automated clustering, an algorithm (k-means clustering; Forgy, 1965) was used, which sorts the normalized data sets according to the similarity of their measured values. The

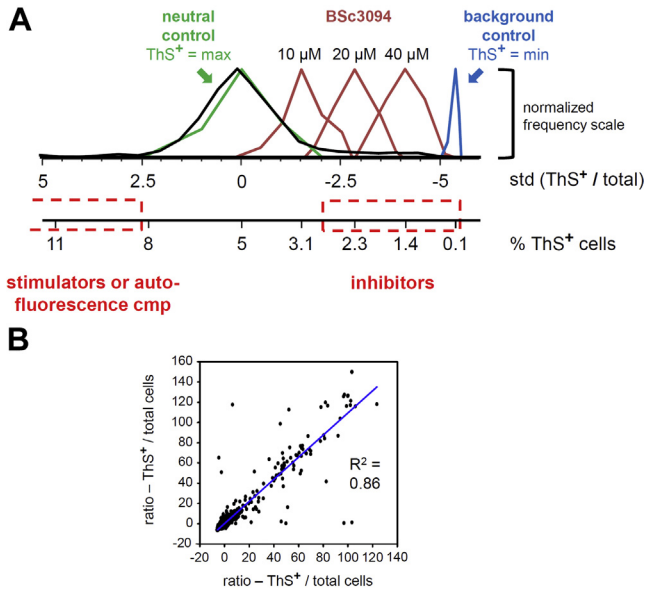

Fig. 2. (A) Distribution and reproducibility of data points. Images of tau$^{RD\Delta K}$ expressing N2a cells were analyzed for the ratio of ThS-positive cells to all cells, and the results were normalized to the mean of the neutral control. Neutral control—green line (+Dox/Cp16, compound untreated; ThS$^+$ cells = max); background control—dark blue line (– Dox/Cp16; compound untreated; ThS$^+$ cells = min); compound samples—black line (+Dox/Cp16; library compound treated); Inhibitor BS3094 samples—brown lines (+Dox/Cp16; +10, 20 and 40 µM BSc3094). On the x-axis, the standard deviation from the neutral control (upper line) and the total percentage of ThS$^+$ cells (lower line) is shown. (B) The reproducibility of 2 independent screening runs over all compounds was up to 86%. (For interpretation of the references to color in this figure legend, the reader is referred to the Web version of this article.)

algorithm assigns a group of data to k virtual centers (x-axis: 10 compound concentration points; y-axis: data for the ratio of ThS$^+$ cells to all cells (Fig. 3A–C) or the total cell count (Fig. 3D and E)) by optimization of the root mean square values. When additional data are included, the k-centers are recalculated. The calculation is repeated until the k-centers no longer change their virtual position. This analysis allowed us to assess the tested compounds as (1) inhibitors, (2) stimulators, or (3) nonresponders (Fig. 3A–C; ratio of ThS$^+$ cells decreasing, increasing, or constant, resp.) and cytotoxic or nontoxic compounds (Fig. 3D and E; cell count decreasing or constant). This identified 54 approved tau aggregation modulating substances (29 inhibitors and 25 stimulators) for tau$^{RD\Delta K}$ expressing N2a cells (Table S1A and S1B).

2.7. Properties of inhibitors, stimulators, and nonresponders

When DR curves of inhibitory compounds are analyzed with regard to the ratio of ThS$^+$ cells (ThS—12 data sets), total cell count (DRAQ5 nuclei staining—6 data sets), and viability (resazurin staining—2 data sets), one can distinguish 3 main categories:

(a) "Classic" inhibition (Fig. 4A)—for these compounds, the inhibitory effect on tau aggregation is very weak at low concentrations similar to the positive control. The effect (decrease of ThS$^+$ cells)—rises with increasing concentrations and reaches a baseline at high compound concentrations. At the same time, the cytotoxicity (cell count) and viability (resazurin) of the cells are hardly affected.
(b) "Highly potent" inhibition (Fig. 4B)—in this class, we found very strong inhibitors of tau aggregation, such that even at low compound concentrations (250 nM), the ratio of ThS$^+$ cells are strongly reduced and in the tested concentration range, the DR curve does not reach the level of the untreated control. To further check these compounds, we performed a similar assay in a concentration range of 400 to 2.5 nM (examples shown in Fig. 5A–C). As in the "classic" compounds, there is no increased cytotoxicity or reduced viability (Fig. 4B).
(c) "Limited concentration" inhibition (Fig. 4C)—some of the tested compounds show a "classic" trend in the DR curve at low and medium concentrations. However, at high concentrations, the curve shows increasing cytotoxicity, as seen by the decreasing viability of the N2a cells. Such compounds are suitable for antiaggregation treatment only in a limited concentration range. Nevertheless, these compounds could be used for cotreatment experiment at medium concentrations to investigate possible synergistic effects of 2 or more compounds.

In the case of stimulators, we found at least 3 classes of compounds that increase the fraction of ThS$^+$ cells. The increase is mainly observed in the induced (by Dox/Cp16) tau$^{RD\Delta K}$ expressing N2a cells. The uninduced cells show only minor increase in the number of ThS$^+$ cells (Fig. S4B), which could be caused by the leakiness of the tau$^{RD\Delta K}$ expression system (note: even uninduced cells show an amount of ~0.1% ThS$^+$ cells; Fig. 2A).

- "Classic" stimulation (Fig. 4D)—at low concentrations, we observe no compound effect and the ThS$^+$ cell ratio is similar to that of the compound-untreated positive control. At higher concentrations, the ThS$^+$ cell fraction rises and reaches a maximum.
- "Highly potent" stimulation (Fig. 4E)—even at the lowest tested compound concentration (250 nM), the ThS$^+$ cell fraction is strongly increased and the DR curve starts far above the level of the compound-untreated control. In such cases, the stimulator compound was retested at a lower concentration range of 400 to 2.5 nM (examples in Fig. 5D–F).
- "Limited concentration" stimulation (Fig. 4F)—some compounds show atypical curve progression at high compound concentrations. In these cases, we observed a constant increase in the amount of ThS$^+$ cells, which collapses at very high concentrations. This phenomenon could be explained by precipitation effects of the compound in the cell medium or the toxication of other cellular components.

As shown before, tau aggregation (on the level of oligomeric and/or fibril aggregates) is toxic for cells. Therefore, it was not surprising that all tested tau aggregation stimulators show cytotoxicity (decreasing cell count and reduced viability (Fig. 4D–F) in a dose-dependent manner).

The DR screening–identified compounds related to the inhibition of 3 major targets led to inhibition of tau aggregation: p38 mitogen-activated protein kinase (p38 MAPK) (7 of 8 compounds in the initial library), vascular endothelial growth factor receptor 1/2 (3 of 8), and TGF (3 of 10). This suggests that the activity of these 3 proteins is permissive or promotes tau aggregation. Conversely, compounds related to histone deacetylases (HDAC) inhibition (16 of 20) led to enhanced tau aggregation, suggesting that HDAC activity is important for suppressing aggregation. A summary of inhibitor and stimulator compounds is given in Table S1A and B.

2.8. Effect of tau modulators on tau transcription

We asked if some of the tested compounds have a direct effect on the tau gene expression level. To clarify this question, we analyzed N2a cell lysates by real-time polymerase chain reaction

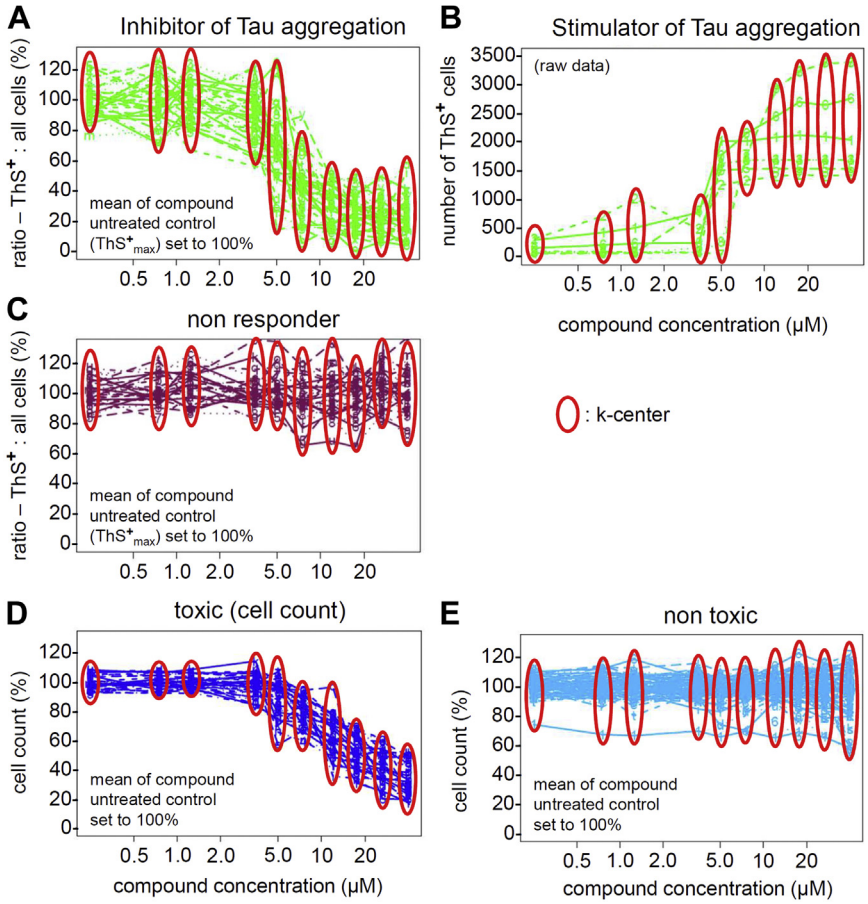

Fig. 3. Clustering analysis of inhibitors (A), stimulators (B), and nonresponders (C) of tau$^{RD\Delta K}$ aggregation in N2a cells and of toxic (D) and nontoxic (E) tau aggregation modulators. Data points were normalized to the neutral control (induced, compound-untreated; ratio of ThS$^+$ to cell count was set to 100% in A and C; total cell count in the neutral control was set to 100% in D and E; raw data for the count of ThS$^+$ cells are shown in B). Red circles represent the virtual k-centers for the cluster analysis. (For interpretation of the references to color in this figure legend, the reader is referred to the Web version of this article.)

(RT-PCR) after 2 days of tau$^{RD\Delta K}$ expression (see Material and Methods 4.8.). This revealed 28 modulators of tau aggregation (10 stimulator and 18 inhibitor compounds), which increased or decreased the amount of ThS$^+$ cells without major changes in tau expression level (Fig. 5 and Table 1). The tau expression levels were normalized by the expression of actin and GAPDH genes (Fig. S5A and B).

2.9. Effect of HDAC inhibitors on tau aggregation

Treatment with HDAC inhibitor compounds led to a strong increase in ThS$^+$ cells, suggestive of a higher rate of tau aggregation. To show this on a greater number of cells, we monitored the increase of tau aggregates over time up to 96 hours of incubation/tau expression (5 runs, up to 100 ThS$^+$ cells). Images were acquired every 90 minutes and the ThS$^+$ cells were identified via their fluorescence intensity, cell size, and cell shape (Fig. 1B–D). This experiment revealed (1) the tau aggregation started reproducibly after 33–34 hours of induction, independently of the presence of the HDAC inhibitor Givinostat (inhibitor of HD1A, HD1B, and HD2) (compare Fig. S4A and B without or with Givinostat) or compound Cp16; (2) treatment with Givinostat (1.2 µM) led to a nearly 7-fold increase in the fraction of ThS$^+$ cells (from ~12% to ~84%, Fig. S4A and B, blue lines) compared to the uninduced control, and 2.5-fold compared to the induced control.

2.10. Target enrichment, molecular pathways, and network analysis

To properly analyze the targets involved in the regulation of the tau aggregation, we first developed a strategy to map the selected and validated small molecules to the potential targets and the corresponding biological pathways. To achieve this goal, we used Ingenuity Pathway Analysis (IPA) software (Qiagen) to first identify the targets annotated to interact with tau (the "prior knowledge targets"). We then analyzed the stimulator and inhibitor hit compounds validated in our DR analyses. For each of the hit compounds, we built a bioactivity list (i.e., the interaction between a compound and targets). To achieve this step, we collected information, using a custom-made python script, for each hit compound from PubChem, ChEMBL, and Protein Data Bank databases to identify the pharmacological targets of each of the hit compounds. Pharmacological targets were then associated to a hit compound only if there were evidences of direct compound-protein interactions (target-type "single protein") and/or confirmatory binding assays including DR data. The obtained target list was called the hit targets. We then merged the prior knowledge targets with the hit targets to identify known players in tau modulation that scored as hits in our screen. Notably, 23 targets (Table S2, supplementary material) of the prior knowledge targets overlap with the inhibitor compounds and one with the stimulator hits. As the selected hits (18 inhibitors and 10 stimulators) have an effect on a potential novel target Nuclear Receptor Co-Repressor1 involved in tau modulation, we then analyzed

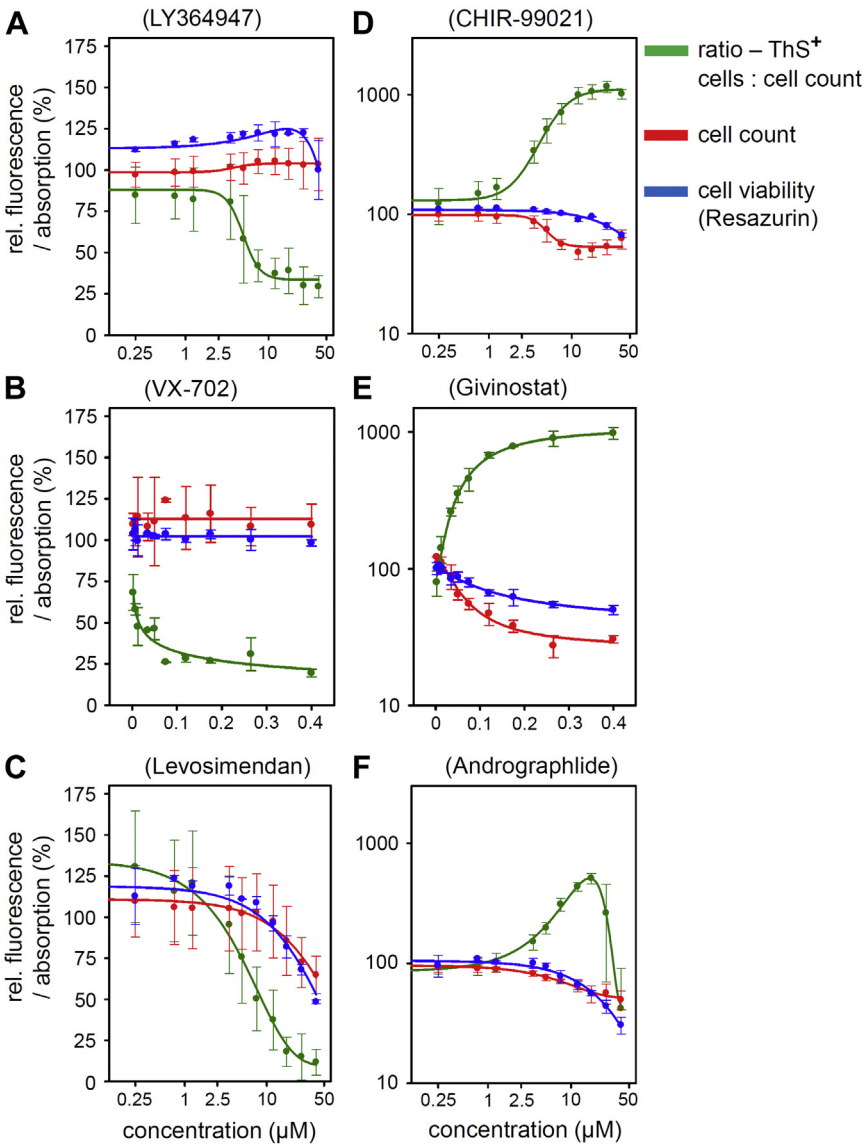

Fig. 4. Examples of tau aggregation inhibitors (A–C) and stimulators (D–F) in secondary dose-dependent screen (40–0.25 µM and 400–2.5 nM), (A) LY364947, (B)VX-702, (C) Levosimendan, (D) CHIR-99021 (CT99021) HCl, (E) Givinostat, (F) Andrographolide. Curve progressions could be classified in "classic" (A and D), "high potential" (B and E), and "limited concentration" (C and F). Three parameters were monitored: The ratio of ThS^{+} cells to all cells (Thioflavin S staining, green line); the total cell count (DRAQ5 staining, red line) and the cell viability by resazurin assay (measurement of the amount of NADH, blue line) in relation to the increasing compound concentration. The induced compound-untreated control (neutral control) was set to 100%. Abbreviation: NADH, nicotinamidadenindinukleotid. (For interpretation of the references to color in this figure legend, the reader is referred to the Web version of this article.)

the small molecules that scored as hits but did not target the prior knowledge network (Fig. 6). The bioactivity analysis of the 18 inhibitor hits identified 225 targets, whereas for the 10 stimulators hits, we identified additional 14 targets (Table S2 supplementary material). We then analyzed the abovementioned targets for gene ontology term enrichment using the BiNGO plugin for Cytoscape (Maere et al., 2005). For our analysis, we chose the hypergeometric test with a Benjamini-Hochberg false discovery rate with a significance level of 0.005.

The gene ontology terms enrichment for the molecular function related to the activator targets elicit the following terms ranking as first ten for *p*-value: (1) deacetylase activity, (2) hydrolase activity (acting on carbon-nitrogen but not peptide bond), (3) hydrolase activity (acting on carbon-nitrogen but not peptide bonds in linear amides), (4) histone deacetylase activity, (5) protein deacetylase activity, (6) protein kinase binding, (7) transcription cofactor activity, (8) transcription repressor binding, (9) kinase binding, (10) protein kinase C binding. For the inhibitor targets, the first ten terms returned were (1) protein kinase activity, (2) phosphotransferase activity (alcohol group as acceptor), (3) protein serine/threonine kinase activity, (4) nucleotide binding, (5) ribonucleotide binding, (6) transferase activity, (7) transferase activity (transferring phosphorus-containing groups), (8) purine nucleotide binding, (9) purine ribonucleotide binding, and (10) adenyl nucleotide binding.

To understand the relevance and the weight of the targets relevant to tau and Alzheimer's disease, we used the IPA software to analyze the inhibitor and activator targets. Using the bioprofile tools of the IPA software, we filtered the identified targets by association to Alzheimer disease or other tauopathies. Notably, of the 225 targets associated with inhibitory drugs, 27 were associated either with tau pathology (Table S3, supplementary material),

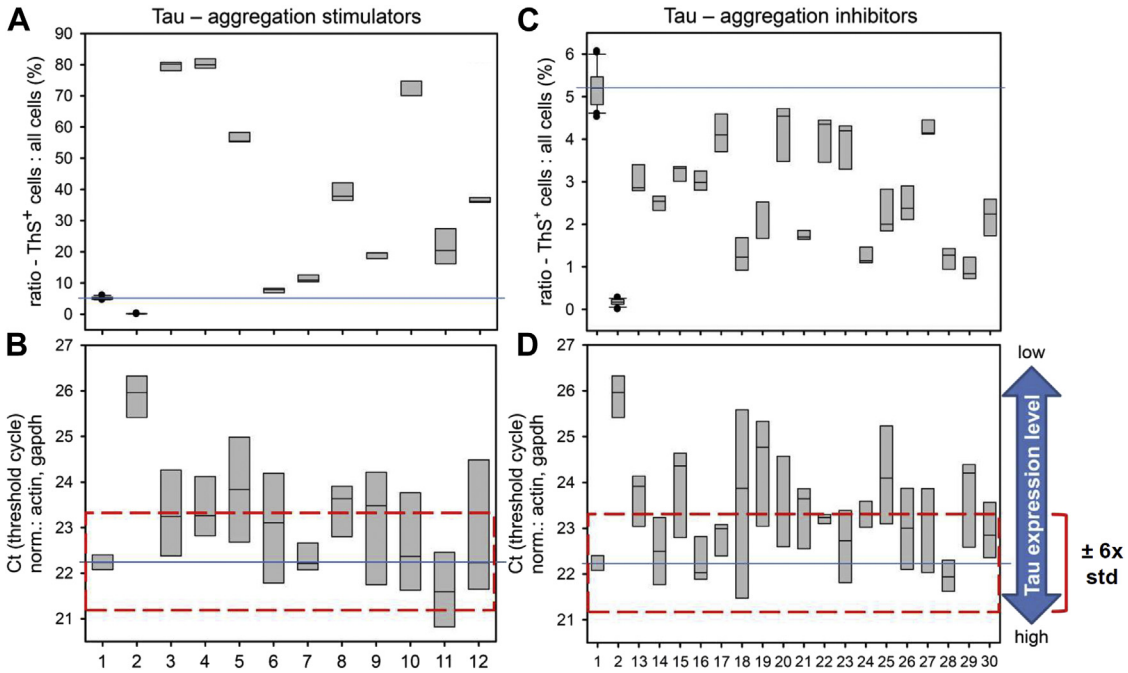

Fig. 5. Comparison of tau expression levels and amounts of ThS$^+$ cells modulated by tau-aggregation stimulatory and inhibitory compounds. Cell lysates of compound-treated tau$^{RD\Delta K}$ expressing N2a cells were used in RT-PCR as template. Shifts in the cycle number reflect the amount of tau gene templates in the sample (earlier PCR signals [SYBR green fluorescence] corresponds with a higher copy number of the gene of interest). Stimulator compounds: (A) ratio of ThS$^+$ cells: all cells, (B) Ct - norm. threshold cycle; Inhibitor compounds: (C) ratio of ThS$^+$ cells: all cells, (D) Ct - norm. threshold cycle. Data for tau expression levels were normalized by the expression levels of the housekeeping genes actin and gapdh (Fig. S5A-B). (For interpretation of the references to color in this figure legend, the reader is referred to the Web version of this article.)

although no association with tauopathies or Alzheimer's disease was found for the remaining targets associated with stimulator drugs (with the exception of the F3 [coagulation factor III] target that is associated with senile plaque formation (McComb et al., 1991)). Of interest, those targets are mainly associated with HDACs.

Table 1
Summary of the tau aggregation modulators (stimulators = 10 [no. 3-12], inhibitors = 18 [no. 13-30]), which shows increase/decrease in the amount of ThS$^+$ cells without affecting the expression level of tau$^{RD\Delta K}$ compared to the compound untreated control

	Stimulator//Inhibitor	Target
1	Neutral control (+Dox, − compound)	
2	Background control (− Dox, − compound)	
3	Mocetinostat (MGCD0103)	HDAC
4	Entinostat (MS-275)	HDAC1/3
5	CUDC-101	HDAC class I/II/EGFR/HER2
6	Diethylstilbestrol	Estrogen receptor
7	Andrographolide	NF-κB/actin
8	CHIR-99021 (CT99021) HCl	GCK-3α/β
9	NCS 207895	MDMX (p53)
10	CI994 (Tacedinaline)	HDAC class 1
11	GSK J4 HCl	Histone demethylase
12	Ricolinostat (ACY-1215)	HDAC6
13	Brivanib Alaninate	VEGFR2
14	SB431542	ALK5
15	Brivanib	VEGFR2
16	Thiazovivin	ROCK
17	Ivermectin	Chloride channel (GluCls) activator
18	LY2228820	p38 MAPK
19	BIRB 796 (Doramapimod)	p38 MAPK
20	Cyproterone acetate	Androgen receptor (AR) antagonist
21	Levosimendan	cTnC
22	DAPT (GSI-IX)	γ-secretase inhibitor
23	Alectinib (CH5424802)	ALK inhibitor
24	A-205804	E-selectin/ICAM-1
25	LY364947	TGF-β-RI
26	LY2109761	TGF-β-RI/II
27	LY411575	γ-Secretase inhibitor
28	Spironolactone	Androgen receptor
29	VX-702	p38α MAPK
30	PP2	Lck/Fyn

3. Discussion

Abnormal changes in tau are characteristic for a number of neurodegenerative diseases (reviews: Goedert et al., 2012; Lee et al., 2001; Wang and Mandelkow, 2016). The most unusual feature is the pathological aggregation of tau, a highly soluble protein in normal conditions. Hence, much effort has gone into the

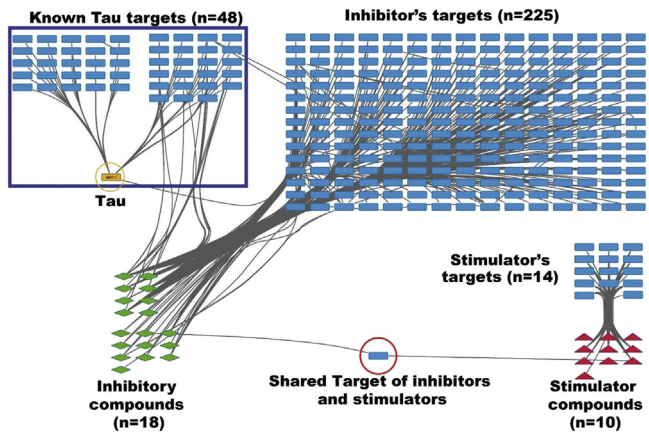

Fig. 6. Network analysis of the targets associated with targets associated with inhibitors, stimulators, and known tau targets. The figure shows the interaction between the protein targets associated with the inhibitors and stimulator compounds and the network of known proteins interacting with tau. Nodes in blue rectangles indicate proteins, red diamond nodes indicate stimulator compounds, and green diamond nodes indicate inhibitor compounds. Edges (gray lines) indicate the connection among different nodes. (For interpretation of the references to color in this figure legend, the reader is referred to the Web version of this article.)

search for inhibitors of tau aggregation in vitro (e.g., Ballatore et al., 2012; Crowe et al., 2013; Pickhardt et al., 2005, 2015; Schafer et al., 2013; Taniguchi et al., 2005; Wischik et al., 1996). Various inhibitor compounds were discovered in the screens, but only few were promising in terms of brain penetrance or safety. A distinct approach is to use cells expressing tau protein harboring some of the pathological changes (e.g., mutations) and screening for compounds to prevent or reverse those changes. Examples of this kind are the screens for kinase inhibitors to reduce hyperphosphorylation (Ahn et al., 2005), for modifiers of tau expression to reduce cellular tau levels (Dehdashti et al., 2013), for microtubule stabilizers to compensate for loss of tau function (Brunden et al., 2017), for modifiers of neuronal tau interactors [e.g., kinase Fyn (Cochran et al., 2014)], or for modifiers of tau aggregation by cellular pathways. In the latter case, the challenge is to achieve robust tau aggregation within the lifetime of a cell (a few days, compared to decades in the brain), observe the development of aggregation and toxicity using suitable readouts, and treat the cells with a library of promising compounds.

Starting from our earlier work on tau aggregation in N2a cell, we describe here the development and validation of such a cellular model system, which allows an automated, image-based data acquisition and data analysis for HCS on pharmacological standards. The HCS assay was miniaturized (384-well format), validated and transferred to a robotic screening platform for fully automated and standardized processing. We screened a library of bioactive annotated compounds and implemented secondary assays. Using automated image routines on an analysis platform (Columbus vers. 2.4.1., Perkin Elmer), we quantified the data further with a high-content assay analyzer (Genedata vers. 11.0.2., Genedata AG) to identify modulators (inhibitors and stimulators) of tau aggregation in tau$^{RD\Delta K}$ expressing N2a cells.

In addition, annotated targets of the bioactive compounds allowed a prediction of intracellular pathways involved in the regulation of tau aggregation. Subsequent secondary DR screens determined the potency and cytotoxicity/viability of the selected hit compounds and identified a condensed set of promising compounds for further testing in cellular and animal models.

This procedure revealed a series of tau-aggregation inhibitors ($n = 18$) and stimulators ($n = 10$) (Table 1) that show reproducible effects on tau$^{RD\Delta K}$ expressing N2a cells in a dose-dependent manner (0.25–40 μM). The computational analysis of the targets related to inhibitor drugs strongly indicated that phosphorylation and kinase activity are emerging as major players among the 225 targets. In addition, 19 of the 27 targets in this group that are associated with Alzheimer's disease and/or tauopathies are kinases.

Among the 18 inhibitors, 2 compounds (LY2228820 and VX-702; both inhibitors of p38 MAPK) are highly potent and active even in a low concentration range (400–2.5 nM). p38 MAPK is capable of increasing diverse features related to AD, such as tau phosphorylation (including potential nonproline phosphorylation sites in tau$^{RD\Delta K}$: T245, S305, and S356, Reynolds et al., 2000), neurotoxicity, neuroinflammation, and synaptic dysfunction. In vivo studies using transgenic mice have demonstrated that p38 MAPK activation is positively correlated with the amount of aggregated tau (Kelleher et al., 2007). It was also shown that p38 MAPK activity was increased in the brains of patients with AD (Robinson et al., 1999) and associated with neurofibrillary pathology in hippocampal and cortical brain regions (Zhu et al., 2000). On the other hand, it is possible that the inhibition of tau aggregation by inhibition of p38 is a more indirect mechanism affecting the phosphorylation of an upstream target. These results suggest that p38 MAPK is significantly—directly or indirectly by other cellular cascades—associated with tau$^{RD\Delta K}$ aggregation and that its inhibition could be a potential strategy to alleviation of tau pathologies by suppressing this phosphorylation (Maphis et al., 2016; Munoz and Ammit, 2010; for review see; Jong and Nam-Jung, 2017).

Recent studies have demonstrated an increasing interest and research activity to elucidate the contribution of the Rho/ROCK signaling pathway to neurodegenerative disease pathogenesis. A large number of downstream targets are phosphorylated by ROCK (e.g., LIM kinase, myosin light chain and myosin light chain phosphatase). They are involved in different biological processes such as the regulation of cell shape and motility, cell survival and apoptosis, and the regulation of the actin-myosin cytoskeleton (Maekawa et al., 1999). ROCK activity leads to an increased number of stable actin filaments and a reduced actin turnover in the cells, thus counteracting cell growth and the regeneration of cell processes like neurites (Endo et al., 2007). Activation of ROCK leads to the phosphorylation of several central regulator proteins finally resulting in decreased cell growth, stress fiber formation, neurite retraction, induction of apoptosis, and inhibition of autophagy. It was shown that expression levels of ROCK, mainly ROCK2, are increased in nervous tissue under different pathological conditions in human samples, especially from patients with neurodegenerative disorders (Herskowitz et al., 2013; for review see; Hensel et al., 2015; Koch et al., 2018). Several reports demonstrated the role of the ROCK-pathway in Aβ synthesis and secretion (Herskowitz et al., 2013; Zhou et al., 2003) and tau hyperphosphorylation (Castro-Alvarez et al., 2011). A recent study showed disease-modifying effects of the clinically approved ROCK inhibitor Fasudil in a Drosophila model of neurodegenerative disorders by reversed rough-eye phenotype and tau levels (Gentry et al., 2016). In this work, we demonstrated the inhibitory effect of the ROCK inhibitor Thiazovivin on tau aggregation in tau$^{RD\Delta K}$ expressing N2a cells. At a concentration of 10 μM in the cell medium, we measured a 40% reduction of ThS^{+} cells with no decrease in the cell count and cell viability after 2 days of tau$^{RD\Delta K}$ expression. Thus, the level of tau expression was not changed compared to the compound untreated control indicating that Thiazovivin does not influence the transcription of the tau gene but reduces the amount of aggregated tau by another mode of action (e.g., activation of the cellular protein degradation machinery).

The stimulation effect of HDAC inhibitors on the tau aggregation in tau$^{RD\Delta K}$ expressing N2a cells raises the question whether tau acetylation of lysine residues would modulate its potential to aggregate. Several sites in the tau$^{RD\Delta K}$ fragment can be acetylated by the histone acetyltransferase p300, the CREB-binding protein or both, leading to an increase in aggregation (Cohen et al., 2011; Cook et al., 2014). In addition, acetylation reduces the degradation of phosphorylated tau (p-tau). Therefore, the accumulation of pathogenic forms of p-tau could reflect its insufficient clearance by proteasome-mediated degradation (Min et al., 2010). tau can also bind directly to the histone-deacetylase HDAC6 and inhibit its activity, which leads to an increase of acetylated tubulin in the cell (Leyk et al., 2015; Perez et al., 2009). Thus, strategies to deacetylate tau could slow down disease progression. The protein deacetylase SIRT1 reduces tau acetylation in vivo. Its functional importance in suppressing the spread of tau pathology was shown in a tauP301S transgenic mice model of neurodegeneration after overexpressing of SIRT1. In contrast, the SIRT1 deficiency leads to exacerbation of premature mortality, synapse loss, and behavioral disinhibition (Min et al., 2018).

16 of 20 (= 80%) HDAC inhibitors present in the initial screening library show the effect of stimulating the cellular aggregation of tau$^{RD\Delta K}$ protein and 5 of them with only minor effect on the tau expression level (Fig. 5; Table 1). In these 5 cases, we observed an increasing amount of ThS^{+} cells up to 13-fold compared to the

compound-untreated control. This suggests that the cellular tau accumulation is mainly due to the lack of cellular degradation rather than to a change in tau$^{RD\Delta K}$ protein expression.

The computational analysis of the targets associated with compounds modulating tau aggregation reveal a number of putative targets related to inhibition of tau aggregation, and on the other hand, a small set of targets that are related to the enhancement of aggregation. With regard to inhibition, the screen revealed 226 targets, of which 197 (~87%) are protein kinases. This class of proteins therefore represents a major pharmacological target for the development of drugs to reduce tau aggregation. Some bias on kinases/phosphorylation might be in part due to the composition of the compound library leaning on kinase inhibitors, but overall, these data also represent the important role of kinases in the regulation of tau aggregation. Our results also show how complex and intricate the kinase network controlling tau is, and we believe that our data will help to address future analysis of the responsible pathways.

With regard to the small molecules that elicit tau aggregation, the analysis of our screen data (within our experimental conditions) strongly point to a role of the HDAC family. This interesting finding opens up a different hypothesis for understanding the regulation of tau degradation and the role of acetylation in this process. On one hand, HDAC inhibitors are considered important for the treatment of Alzheimer's disease. HDAC inhibitors such as Trichostatin A, phenylbutyrate, valproate (Depakote), or SAHA (Vorinostat) have been shown to ameliorate memory function in AD mouse models (Benito et al., 2015; Govindarajan et al., 2013). The memory improvement seems to be grounded on the effects of HDAC inhibitors on synaptic plasticity, whereas none of the inhibitors resulted in altered amyloid deposition. Another mechanism of the HDACs could be due to the regulation of chromatin and gene expression or their effect on estrogen receptors. For example, Trichostatin A, a potent HDAC inhibitor, strongly decreases ERα expression in a dose-dependent manner (for review, see Margueron et al., 2004).

On the other hand, we observed that HDAC inhibitors caused an increase in tau aggregation. If interpreted as a direct interaction, it would imply that increased acetylation of tau promotes its aggregation. This is analogous to the notion that increased tau phosphorylation increases aggregation, suggesting that both posttranslational modifications enhance the pathogenicity of tau. Thus, our data can contribute in the further development of therapeutic strategies addressing aggregation. It should be stressed that our data have been obtained in an in vitro system with a truncated form of tau, that is, the repeat domain responsible for aggregation. The effects we obtained on tau aggregation should therefore have a bearing on the design of clinical trials using HDAC inhibitors.

4. Materials and methods

4.1. Cell culture, treatment

N2atau$^{RD\Delta K}$ cells were cultured in Minimum Essential Medium Eagle medium (MEM, Sigma, M4655, Lot. RNBD5742) with addition of fetal bovine serum (FCS, BioChrom, S 0115, Lot. 1107A) and MEM nonessential amino acids (PAA, M11-003). For the screening procedure, the medium and serum were always used from the same lots. Cell selection was done with the antibiotics Geneticin (G418, Biochrom, A291-25) at 600 μg/mL and Hygromycin B (Invitrogen, 10687-010) at 100 μg/mL. For the splitting procedure, the cells were washed once with Dulbecco's phosphate-buffered saline (Sigma/D8537) and then trypsinized with a Trypsin-EDTA-Solution (Sigma, T3924) for 2:30 minutes at 37 °C. The cell density and quality were measured with a cell viability analyzer (Vi-Cell XR, Beckman Coulter).

4.2. Compounds

We tested 1649 bioactive drugs from a Selleckchem library (http://www.selleckchem.com) including 850 US Food and Drug Administration–approved compounds. Possible targets and affected pathways of the compounds were annotated by several drug databases (see 4.9)

4.3. Screening setup, assays

For screening experiments, the N2atau$^{RD\Delta K}$ cells were seeded on 384-well plates (Perkin Elmer, 6007550 TC; Greiner, CUSG77540) at a density of 6000 cells/well using a Multidrop system (Thermo Scientific). Cells were treated with compounds in a concentration range of 2.5 nM–40 μM in a fully automated system and activated with 2.5 μg/mL doxycycline (Sigma, D9891) and 5 μM of compound Cp16 (Senexis, Ballatore et al., 2012). The TAI BSc3094 (Pickhardt et al., 2007) was used as control at 10–40 μM. Cellular aggregates of tau$^{RD\Delta K}$ were stained by Thioflavin S (Sigma, T-1892), which were added from the beginning at 12 μM (0.0005%). The incubation and tau expression time was 48 hours. In case of viability testing, the cells were treated at hour 47 with 5 μM resazurin (Sigma, R7017) for 1 hour at 37 °C before measurement at 595 nm (exc. 535 nm) with a SpectraMax Paradigm (Molecular Devices). Finally, the cells were fixed with 3.7% FA (Sigma, F1635), and cell nuclei were stained with DRAQ5 (1:3000, BioStatus DR51000) in phosphate-buffered saline for 15 minutes at 37 °C and overnight incubation at 4 °C.

4.4. Image analysis

Image acquisition was done by a Voyager 6000 system for 3 wavelength parameters—(a) exc. 488 nm → em. 525/50 nm (cellular tau aggregates, "green channel"), (b) exc. 405 nm → em. 525/50 nm (identification of autofluorescence compounds, "white channel"), and (c) exc. 635 nm → em. 730/140 nm (identification of cellular nuclei, "red channel"). For each well, 5 regions were documented corresponding to 31.25% of the well surface. After acquisition, all image data were uploaded to an analysis platform (Columbus vers. 2.4.1, Perkin Elmer) for automated cell object detection and classification into ThS-positive and ThS-negative cells. More precisely, the "FindCells Method B" module was applied on the DRAQ5 channel to identify cell candidates. Valid cells were selected from candidates by morphological properties (96 μm^2 < area <665 μm^2, width/length >0.305). Cell objects were finally classified into ThS-negative and ThS-positive by applying a mean ThS intensity threshold (>840 a.u. for positive cells). A small fraction of tau aggregates did not overlap with the cell region (DRAQ5 intensity <1322 a.u.), presumably because the nucleus was lost in these cases. These aggregates were detected with the "FindCells Method C" module and counted as ThS-positive cells. To match the picture analysis of biophysical parameters (toxicity, number of ThS-positive cells) with the respective compound treatment, image analysis results were transferred to a high-content assay analyzer (Genedata vers. 11.0.2., Genedata AG).

4.5. Cluster analysis

Using a k-means clustering algorithm, the tested compounds were classified into subgroups regarding their inhibiting or activating effects on tau aggregation and their cytotoxicity. The algorithm sorted the normalized data sets with regard to the similarity of their measured values and assigned a group of data to k (cluster)

virtual centers by optimizing the root mean square values. When additional data were included, the k-centers were recalculated till the k-centers no longer changed their positions.

4.6. Live imaging of N2atau$^{RD\Delta K}$ cells

N2atau$^{RD\Delta K}$ cells were seeded on 384-well plates at 6000 cells/well. Expression of tau protein was induced by doxycycline (2.5 μg/mL) ± Cp16 (5 μM), and cells were incubated for 96 hours in a 5% CO_2 humidity atmosphere in the presence of 12 μM Thioflavin S to stain cellular aggregates of tau$^{RD\Delta K}$. To measure the effect of HDAC inhibitors on the kinetics of tau-aggregation, 1.2 μM Givinostat was added. Images were acquired every 90 minutes (Voyager 6000) and the count of ThS-positive cells was plotted against the incubation time.

4.7. RT-PCR on compound-treated N2atauR$^{D\Delta K}$ cells

For the real-time one-step RT-PCR analysis from cultured cells without RNA purification, the FastLane Cell SYBR Green Kit (Qiagen, Cat No./ID: 216213) was used according to the manufacturer's instructions. N2atau$^{RD\Delta K}$ cells were cultured as described previously (section 4.1) in the presence of 10 μM compound. After the incubation/tau-expression period, the cells were washed once with FCW (cell wash buffer for effective removal of extracellular contaminants) buffer and then lysed for 5–10 minutes at room temperature (FCPL [component of cell processing mix to allow efficient lysis of cultured cells and RNA stabilization] + FCPM [component of cell processing mix to enhance performance] + gDNA wipeout buffer; 12.5 μL in total/well), and 3 μL of the lysate was transferred to the RT-PCR sample, or the whole lysates were transferred into safe-seal tubes for storage at −80 °C.

The PCR (20 μL/well) was composed as follows: 10 μL 2× QuantiTect SYBR Green RT-PCR master mix + 1.6 μL forward_primer (100 pmol/μL = 100 μM; 8 μM end concentration) + 1.6 μL reverse_primer (100 pmol/μL = 100 μM; 8 μM end concentration) + 0.2 μL QuantiTect RT mix +1 μL 5× Q-Solution + 3 μL FastLane cell lysate and 2.6 μL RNase-free water to a total volume of 20 μL. PCR was performed in an RT-PCR 7900 HT Fast Real Time (Applied Biosystems) with a 384-well thermo block. As PCR program, a standard protocol was used: Step 1—2:00 minutes 50 °C; step 2—10:00 minutes 95 °C; step 3 (40 times repeated)—0:15 minutes 95 °C + 1:00 minutes 60 °C; step 4—0:15 minutes 95 °C + 0:15 minutes 60 °C. To detect mRNA of tau$^{RD\Delta K}$ and selected housekeeping genes, we used the following primer: tau—IK11n (5'-CATCGATATGCAGACAGCCC-3') + IK12n (5'-CGTCGACGGATCC-TATTCAA-3'); β-actin—β-actin_for (5′-AGGCCAACCGTGAAAA-GATG-3′) + β-actin_rev (5′-GATGGCTACGTACATGGCTG-3′); Gapdh—Gapdh_for (5′-AAAAGGGTCATCATCTCCGC-3′) + Gapdh_-rev (5′-ATTTCTCGTGGTTCACACCC-3′). The RT-PCR was performed in a 384-well format with specially designed plates (Applied Biosystems; MicroAmp Optical 384-Well Reaction Plate, no. 4309849; MicroAmp Optical Adhesive Film, no. 4360954).

Disclosure

The authors have no actual or potential conflicts of interest.

Acknowledgements

This research was funded by DZNE, MPG, the Katharina-Hardt Foundation, and an iDSN and HUMIT grant (BMBF). The authors thank Dr Jacek Biernat and Sabrina Hübschmann for generation of the cell line, Dr Bruno Bulic for the synthesis of compound BSc3094, Dr Wera Roth and Dr David Hecker for the support in data analysis and network reconstruction, and Dr Eva-Maria Mandelkow for stimulating discussions.

Appendix A. Supplementary data

Supplementary data to this article can be found online at https://doi.org/10.1016/j.neurobiolaging.2018.11.026.

References

Ahn, J.S., Radhakrishnan, M.L., Mapelli, M., Choi, S., Tidor, B., Cuny, G.D., Musacchio, A., Yeh, L.A., Kosik, K.S., 2005. Defining Cdk5 ligand chemical space with small molecule inhibitors of tau phosphorylation. Chem. Biol. 12, 811–823.

Ballatore, C., Crowe, A., Piscitelli, F., James, M., Lou, K., Rossidivito, G., Yao, Y., Trojanowski, J.Q., Lee, V.M., Brunden, K.R., Smith 3rd, A.B., 2012. Amino-thienopyridazine inhibitors of tau aggregation: evaluation of structure-activity relationship leads to selection of candidates with desirable in vivo properties. Bioorg. Med. Chem. 20, 4451–4461.

Benito, E., Urbanke, H., Ramachandran, B., Barth, J., Halder, R., Awasthi, A., Jain, G., Capece, V., Burkhardt, S., Navarro-Sala, M., Nagarajan, S., Schütz, A.L., Johnsen, S.A., Bonn, S., Lührmann, R., Dean, C., Fischer, A., 2015. HDAC inhibitor-dependent transcriptome and memory reinstatement in cognitive decline models. J. Clin. Invest. 125, 3572–3584.

Bulic, B., Pickhardt, M., Khlistunova, I., Biernat, J., Mandelkow, E.M., Mandelkow, E., Waldmann, H., 2007. Rhodanine-based tau aggregation inhibitors in cell models of tauopathy. Angew. Chem. Int. Ed. Engl. 46, 9215–9219.

Bulic, B., Pickhardt, M., Mandelkow, E., 2013. Progress and developments in tau aggregation inhibitors for Alzheimer disease. J. Med. Chem. 56, 4135–4155.

Brunden, K.R., Lee, V.M., Smith 3rd, A.B., Trojanowski, J.Q., Ballatore, C., 2017. Altered microtubule dynamics in neurodegenerative disease: therapeutic potential of microtubule-stabilizing drugs. Neurobiol. Dis. 105, 328–335.

Castro-Alvarez, J.F., Gutierrez-Vargas, J., Darnaudery, M., Cardona-Gomez, G.P., 2011. ROCK inhibition prevents tau hyperphosphorylation and p25/CDK5 increase after Global Cerebral Ischemia. Behav. Neurosci. 125, 465–472.

Cochran, J.N., Diggs, P.V., Nebane, N.M., Rasmussen, L., White, E.L., Bostwick, R., Maddry, J.A., Suto, M.J., Roberson, E.D., 2014. AlphaScreen HTS and live-cell bioluminescence resonance energy transfer (BRET) assays for identification of Tau-Fyn SH3 interaction inhibitors for Alzheimer disease. J. Biomol. Screen. 19, 1338–1349.

Cohen, T.J., Guo, J.L., Hurtado, D.E., Kwong, L.K., Mills, I.P., Trojanowski, J.Q., Lee, V.M., 2011. The acetylation of tau inhibits its function and promotes pathological tau aggregation. Nat. Commun. 2, 252.

Cook, C., Carlomagno, Y., Gendron, T.F., Dunmore, J., Scheffel, K., Stetler, C., Davis, M., Dickson, D., Jarpe, M., DeTure, M., Petrucelli, L., 2014. Acetylation of the KXGS motifs in tau is a critical determinant in modulation of tau aggregation and clearance. Hum. Mol. Genet. 23, 104–116.

Crowe, A., James, M.J., Lee, V.M., Smith 3rd, A.B., Trojanowski, J.Q., Ballatore, C., Brunden, K.R., 2013. Aminothienopyridazines and methylene blue affect Tau fibrillization via cysteine oxidation. J. Biol. Chem. 288, 11024–11037.

Dehdashti, S.J., Zheng, W., Gever, J.R., Wilhelm, R., Nguyen, D.T., Sittampalam, G., McKew, J.C., Austin, C.P., Prusiner, S.B., 2013. A high-throughput screening assay for determining cellular levels of total tau protein. Curr. Alzheimer Res. 10, 679–687.

Dennissen, F.J., Anglada-Huguet, M., Sydow, A., Mandelkow, E., Mandelkow, E.M., 2016. Adenosine A1 receptor antagonist rolofylline alleviates axonopathy caused by human TauΔK280. Proc. Natl. Acad. Sci. U. S. A. 113, 11597–11602.

Endo, M., Ohashi, K., Mizuno, K., 2007. LIM kinase and slingshot are critical for neurite extension. J. Biol. Chem. 282, 13692–13702.

Fatouros, C., Pir, G.J., Biernat, J., Koushika, S.P., Mandelkow, E., Mandelkow, E.M., Schmidt, E., Baumeister, R., 2012. Inhibition of tau aggregation in a novel Caenorhabditis elegans model of tauopathy mitigates proteotoxicity. Hum. Mol. Genet. 21, 3587–3603.

Forgy, E.W., 1965. Cluster analysis of multivariate data: efficiency versus interpretability of classifications. Biometrics 21, 768–769.

Gentry, E.G., Henderson, B.W., Arrant, A.E., Gearing, M., Feng, Y., Riddle, N.C., Herskowitz, J.H., 2016. Rho kinase inhibition as a therapeutic for progressive supranuclear palsy and corticobasal degeneration. J. Neurosci. 36, 1316–1323.

Goedert, M., Ghetti, B., Spillantini, M.G., 2012. Frontotemporal dementia: implications for understanding Alzheimer disease. Cold Spring Harb Perspect. Med. 2, a006254.

Govindarajan, N., Rao, P., Burkhardt, S., Sananbenesi, F., Schlüter, O.M., Bradke, F., Lu, J., Fischer, A., 2013. Reducing HDAC6 ameliorates cognitive deficits in a mouse model for Alzheimer's disease. EMBO Mol. Med. 5, 52–63.

Hensel, N., Rademacher, S., Claus, P., 2015. Chatting with the neighbors: crosstalk between Rho-kinase (ROCK) and other signaling pathways for treatment of neurological disorders. Front. Neurosci. 9, 198.

Herskowitz, J.H., Feng, Y., Mattheyses, A.L., Hales, C.M., Higginbotham, L.A., Duong, D.M., Montine, T.J., Troncoso, J.C., Thambisetty, M., Seyfried, N.T., Levey, A.I., Lah, J.J., 2013. Pharmacologic inhibition of ROCK2 suppresses amyloid-β production in an Alzheimer's disease mouse model. J. Neurosci. 33, 19086–19098.

Jong, K.L., Nam-Jung, K., 2017. Recent advances in the inhibition of p38 MAPK as a potential strategy for the treatment of Alzheimer's disease. Molecules 22, 1287.

Kelleher, I., Garwood, C., Hanger, D.P., Anderton, B.H., Noble, W., 2007. Kinase activities increase during the development of tauopathy in htau mice. J. Neurochem. 103, 2256–2267.
Khlistunova, I., Biernat, J., Wang, Y., Pickhardt, M., von Bergen, M., Gazova, Z., Mandelkow, E., Mandelkow, E.M., 2006. Inducible expression of Tau repeat domain in cell models of tauopathy: aggregation is toxic to cells but can be reversed by inhibitor drugs. J. Biol. Chem. 281, 1205–1214.
Koch, J.C., Tatenhorst, L., Roser, A.E., Saal, K.A., Tönges, L., Lingor, P., 2018. ROCK inhibition in models of neurodegeneration and its potential for clinical translation. Pharmacol. Ther. 189, 1–21.
Lee, V.M., Goedert, M., Trojanowski, J.Q., 2001. Neurodegenerative tauopathies. Annu. Rev. Neurosci. 24, 1121–1159.
Leyk, J., Goldbaum, O., Noack, M., Richter-Landsberg, C., 2015. Inhibition of HDAC6 modifies tau inclusion body formation and impairs autophagic clearance. J. Mol. Neurosci. 55, 1031–1046.
Maekawa, M., Ishizaki, T., Boku, S., Watanabe, N., Fujita, A., Iwamatsu, A., Obinata, T., Ohashi, K., Mizuno, K., Narumiya, S., 1999. Signaling from Rho to the actin cytoskeleton through protein kinases ROCK and LIM-kinase. Science 285, 895–898.
Maere, S., Heymans, K., Kuiper, M., 2005. BiNGO: a Cytoscape plugin to assess overrepresentation of Gene Ontology categories in biological networks. Bioinformatics 21, 3448–3449.
Maphis, N., Jiang, S., Xu, G., Kokiko-Cochran, O.G., Roy, S.M., Van Eldik, L.J., Watterson, D.M., Lamb, B.T., Bhaskar, K., 2016. Selective suppression of the α isoform of p38 MAPK rescues late-stage tau pathology. Alzheimers Res. Ther. 8, 54.
Margueron, R., Duong, V., Castet, A., Cavaillès, V., 2004. Histone deacetylase inhibition and estrogen signaling in human breast cancer cells. Biochem. Pharmacol. 68, 1239–1246.
McComb, R.D., Miller, K.A., Carson, S.D., 1991. Tissue factor antigen in senile plaques of Alzheimer's disease. Am. J. Pathol. 139, 491–494.
Min, S.W., Cho, S.H., Zhou, Y., Schroeder, S., Haroutunian, V., Seeley, W.W., Huang, E.J., Shen, Y., Masliah, E., Mukherjee, C., Meyers, D., Cole, P.A., Ott, M., Gan, L., 2010. Acetylation of tau inhibits its degradation and contributes to tauopathy. Neuron 67, 953–966.
Min, S.W., Sohn, P.D., Li, Y., Devidze, N., Johnson, J.R., Krogan, N.J., Masliah, E., Mok, S.A., Gestwicki, J.E., Gan, L., 2018. SIRT1 deacetylates tau and reduces pathogenic tau spread in a mouse model of tauopathy. J. Neurosci. 38, 3680–3688.
Morris, M., Maeda, S., Vossel, K., Mucke, L., 2011. The many faces of tau. Neuron 70, 410–426.
Munoz, L., Ammit, A.J., 2010. Targeting p38 mapk pathway for the treatment of Alzheimer's disease. Neuropharmacology 58, 561–568.
Perez, M., Santa-Maria, I., Gomez de Barreda, E., Zhu, X., Cuadros, R., Cabrero, J.R., Sanchez-Madrid, F., Dawson, H.N., Vitek, M.P., Perry, G., Smith, M.A., Avila, J., 2009. Tau – an inhibitor of deacetylase HDAC6 function. J. Neurochem. 109, 1756–1766.
Pickhardt, M., Biernat, J., Hübschmann, S., Dennissen, F.J.A., Timm, T., Aho, A., Mandelkow, E.M., Mandelkow, E., 2017. Time course of Tau toxicity and pharmacologic prevention in a cell model of Tauopathy. Neurobiol. Aging 57, 47–63.
Pickhardt, M., Gazova, Z., von Bergen, M., Khlistunova, I., Wang, Y., Hascher, A., Mandelkow, E.M., Biernat, J., Mandelkow, E., 2005. Anthraquinones inhibit tau aggregation and dissolve Alzheimer paired helical filaments *in vitro* and in cells. J. Biol. Chem. 280, 3628–3635.
Pickhardt, M., Larbig, G., Khlistunova, I., Coksezen, A., Meyer, B., Mandelkow, E.M., Schmidt, B., Mandelkow, E., 2007. Phenylthiazolyl-hydrazide and its derivatives are potent inhibitors of tau aggregation and toxicity *in vitro* and in cells. Biochemistry 46, 10016–10023.
Pickhardt, M., Neumann, T., Schwizer, D., Callaway, K., Vendruscolo, M., Schenk, D., St George-Hyslop, P., Mandelkow, E.M., Dobson, C.M., McConlogue, L., Mandelkow, E., Toth, G., 2015. Identification of small molecule inhibitors of tau aggregation by targeting monomeric tau as a potential therapeutic approach for tauopathies. Curr. Alzheimer Res. 12, 814–828.
Reynolds, C.H., Betts, J.C., Blackstock, W.P., Nebreda, A.R., Anderton, B.H., 2000. Phosphorylation sites on tau identified by nanoelectrospray mass spectrometry: differences in vitro between the mitogen-activated protein kinases ERK2, c-Jun N-terminal kinase and P38, and glycogen synthase kinase-3beta. J. Neurochem. 74, 1587–1595.
Robinson, K.A., Stewart, C.A., Pye, Q.N., Nguyen, X., Kenney, L., Salzman, S., Floyd, R.A., Hensley, K., 1999. Redox-sensitive protein phosphatase activity regulates the phosphorylation state of p38 protein kinase in primary astrocyte culture. J. Neurosci. Res. 55, 724–732.
Schafer, K.N., Cisek, K., Huseby, C.J., Chang, E., Kuret, J., 2013. Structural determinants of Tau aggregation inhibitor potency. J. Biol. Chem. 288, 32599–32611.
Taniguchi, S., Suzuki, N., Masuda, M., Hisanaga, S., Iwatsubo, T., Goedert, M., Hasegawa, M., 2005. Inhibition of heparin-induced tau filament formation by phenothiazines, polyphenols, and porphyrins. J. Biol. Chem. 280, 7614–7623.
Wang, Y., Mandelkow, E., 2016. Tau in physiology and pathology. Nat. Rev. Neurosci. 17, 5–21.
Wischik, C.M., Edwards, P.C., Lai, R.Y., Roth, M., Harrington, C.R., 1996. Selective inhibition of Alzheimer disease-like tau aggregation by phenothiazines. Proc. Natl. Acad. Sci. U. S. A. 93, 11213–11218.
Zhou, Y., Su, Y., Li, B., Liu, F., Ryder, J.W., Wu, X., Gonzalez-DeWhitt, P.A., Gelfanova, V., Hale, J.E., May, P.C., Paul, S.M., Ni, B., 2003. Nonsteroidal anti-inflammatory drugs can lower amyloidogenic Abeta42 by inhibiting Rho. Science 302, 1215–1217.
Zhu, X.W., Rottkamp, C.A., Boux, H., Takeda, A., Perry, G., Smith, M.A., 2000. Activation of p38 kinase links tau phosphorylation, oxidative stress, and cell cycle-related events in Alzheimer disease. J. Neuropathol. Exp. Neurol. 59, 880–888.